Automatic Targeting of the Subthalamic Nucleus for Deep Brain Stimulation

Ricardo Miguel de Oliveira Moreira
ricardo.moreira@tecnico.ulisboa.pt

Instituto Superior Técnico, Universidade de Lisboa, Lisboa, Portugal

November 2016

***Abstract* —Deep brain stimulation, which works with the emission of high frequency pulses in specific brain structures, is a procedure used for the treatment of Parkinson's disease. During the planning of the surgery of the electrode implants, the stimulation target must be located with extreme precision. The target selected for the treatment of Parkinson's disease is usually the subthalamic nucleus and its location is normally obtained by iterative methods based on the observation of the brain images. The purpose of this work is to create a method for its automatic targeting. Two approaches are presented in this work. The first one considers a collection of anatomical measurements of the brain and uses them to predict the location of the implanted electrodes. The second one has the same working basis, however it uses a set of extracted features from small volumes of the medical image, located around the mesencephalon and the diencephalon. The errors obtained for both the approaches were very close to those from the surgical planning, where predictions were made manually, for the same group of patients used in the models, by the medical team from Hospital de Santa Maria (1.55 and 2.67 millimeters for the component orthogonal to the electrode trajectory and for the component within the trajectory, respectively). The minimum errors obtained with the predictive models were 1.36 (orthogonal) and 2.28 (within trajectory) millimeters.**

***Keywords*—Automatic targeting, subthalamic nucleus, deep brain stimulation, Parkinson's disease, support vector machine, linear regression**

I. Introduction

DEEP brain stimulation (DBS) is a technique used for the treatment of some neurologic dysfunctions such as Parkinson's disease (PD) [1]. It works through the emission of high frequency pulses in specific areas of the brain which vary according the disease being treated [2].

For the DBS technique to be applied, it is necessary a surgical intervention which consists in the insertion of electrodes on the stimulation targets. This surgery must be done with the maximum precision possible since the dimensions of those stimulation targets are very reduced and the number of safe trajectories for the electrodes is limited.

The most common target for the treatment of PD's symptoms is the subthalamic nucleus (STN) [3]. This structure is found in both cerebral hemispheres, therefore, the implantation of the electrodes is, generally, bilateral and both subthalamic nucleus remain under stimulation after the intervention.

Due to the similarity between the density of the STN and the surrounding structures, it is rarely possible to identify them on the conventional medical images [4]. This is the main difficulty found during the planning of the electrodes' implantation. Thus, the methods that are most used to locate the STN are based on statistical atlas which provide a set of functional coordinates relative to the middle commissural point (MCP-based)[5, 6, 7, 8, 9, 10]. From these coordinates it is obtained a first estimation of the STN's location which will then be adjusted trough iterative methods based on the observation of the position of the surrounding structures.

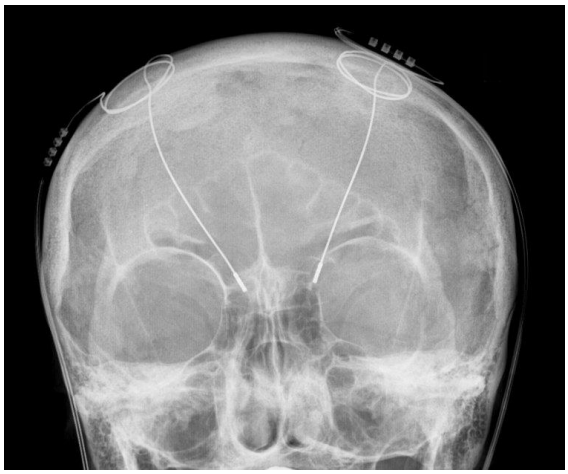

Fig. 1. DBS electrodes visible in X-ray image [17]

During the surgical procedure, the predicted location of the STN, obtained during planning, is adjusted by the micro electrophysiological recording and by macro stimulation tests. These two procedures are executed with a set of 5 microelectrodes, which are introduced through the planned trajectory. One of the electrodes is central and the remaining are separated by 2mm gaps in lateral, medial, anterior and posterior directions. After the electrophysiological stimulation tests (executed in various spots of the various trajectories that were chosen based on the recordings) it is elected the best stimulation spot which will be the target of the treatment. The definitive electrode is then introduced trough the trajectory of the chosen spot and, after the patient recovery, a stimulation test is performed to the various poles located on the tip of the electrode. The goal of this test is to find which stimulation contact provides the best clinical results. The position of the

Fig. 3. 5 Microelectrode configuration [14]

active contact will be considered as the best location found for that patient.

The methods for the automatic prevision of the STN's location already validated are based on image registration tools to find, in a new patient, the analog of the stimulation spots already implemented in other patients [4, 11, 12]. For the implementation of this method is necessary, at first, to find the coordinates of the stimulation spots of a group of patients on which the electrodes had already been implanted. The coordinates of those stimulation spots are obtained through medical images (generally CT) acquired after surgery, on which is possible to see the implanted electrodes. The second step is the registration of those patients' MRIs on the new patient. On these MRIs, the STN's location, obtained during the first step, was previously marked. This way, the patient will have registered on his MRI a cloud of stimulation spots representing the results obtained in previous interventions. Thus, the method estimation of the STN's location corresponds to that cloud's centroid.

The goal of the study presented is to propose and validate an automatic method for the location of the STN based on a predictive model that uses the information of the patient's encephalic image. The motivation for the creation of a model of this kind originated from the conviction that the variability of the STN's positioning is somehow related to the variation in size and location of other structures visible in the medical images. The proposed models, receive as an input, the information related to the encephalic image of a patient and provide as an output, the 3 coordinates of STN's location relatively to the mid-commissural point (MCP). The two main approaches proposed will be tested with various learning methods and various data combinations. The difference between these two approaches is the type of information acquired from the patient's MRI. The measurements' approach considers a set of anatomical dimensions obtained in the MRI. The second approach considers, starting from a set of small cubic volumes located around the ventricular system, mesencephalon and diencephalon, a set of image features such

Fig. 2. Zoom in the DBS electrode tip. The four contacts are responsible for the stimulation. Each contact has the diameter of 1mm and 1.5mm of height

as the spatial average of the voxels' intensity values and the 3 averages of the directional gradients obtained from each voxel. This last approach was named features' approach. These two types of approaches were tested considering 2 learning methods: linear regression (LR) and nonlinear regression based on a support vector machine (SVM). Due to the over dimensionality of the entry data considered for both models, two kinds of methods were applied to reduce the data dimensionality – feature selection and feature extraction – in order to obtain more precise models. For the features selection a wrapper method was implemented, using a genetic algorithm. The feature extraction was implemented trough a principal component analysis (PCA).

Another important aspect considered was the brain shift effect, a phenomenon that occurs with the loss of liquor during the surgical procedure. That loss translates in a weakening of the structural support of the brain which, after some time, starts to suffer small deformations. Therefore, due to the bilateralism of the implants, that happen sequentially, when the second implant is introduced the brain has suffered a more significant deformation. Thus, the deviation between the estimated target, during the planning, and the final stimulation target is larger for the second implant. As such, from the collected data a selection of the first implants was preformed, so that some models consider only these and other consider both sides of implants.

II. Materials and Methods

A. Data

In this study, a set of 18 patients with PD, whose bilateral implants were performed from 2006 to 2012, were considered (36 implantations). Data form all the surgery plans were gathered containing functional coordinates of the estimated STN's location. Information regarding the side order of each implant (left or right) was gathered as well.

T1-weighted magnetic resonances were generally acquired with TR 24.9ms, TE 1.6ms, 256 x 256 x 100 voxels, a resolution of 1.0156 x 1.0156 x 2 mm^3 in a 1.5T scanner. The computerized tomography exams were mainly acquired at kVp=120, exposure 315mAs and 512x512 pixels. In-plane resolution and slice thickness were, respectively, 0.5391x0.5391 mm^2 and 2mm.

B. Measurements Model

The information used in the first model proposed was a set of 10 anatomical dimensions that were measured from the T1-weighted MRI of each patient. To create this model, it was required to gather this dimensions from a set of implanted patients. These anatomical measurements were suggested by the neurosurgery team from Hospital de Santa Maria. The 10 measurements were (see numbers in figure 4 bellow):

- Distance between anterior and posterior commissures (1)
- Left and right bi-ventricular axis (2 and 3, respectively) – It is the distance between the 3rd ventricle floor and the lateral side of the frontal horn of the respective lateral ventricle. This distance is measured in the coronal plane that contains the mid-commissural point (MCP).
- Inter insular lobe distance (4) – It is the distance that goes from the left to the right insular lobe measured over a horizontal line that intersects the MCP, in the coronal plane that also contains it.
- Third ventricle width (5) – Distance between the lateral walls of the third ventricle measured in the axial plane that contains the MCP over a lateral-medial line that also crosses the MCP.
- Third ventricle height (6) – Distance between the floor and the roof of the third ventricle, measured in the coronal plane that contains the MCP over a vertical line that also intersects it.
- Corpus Callosum's chord (7) – The longest distance, measured in the sagittal plane that contains the MCP, that separates the posterior side of the genu of the corpus callosum and the anterior side of the splenium.
- Corpus Callosum's vertical axis (8) – Distance between the MCP and the inferior side of the Corpus Callosum trunk, measured over a vertical line in the sagittal plane that contains the MCP.
- Distance between the outermost portions of the frontal horns of the lateral ventricles, measured in the coronal plane that contains the MCP (9).
- Distance between the innermost portions of the temporal horns of the lateral ventricles, measured in the coronal plane containing the MCP (10).

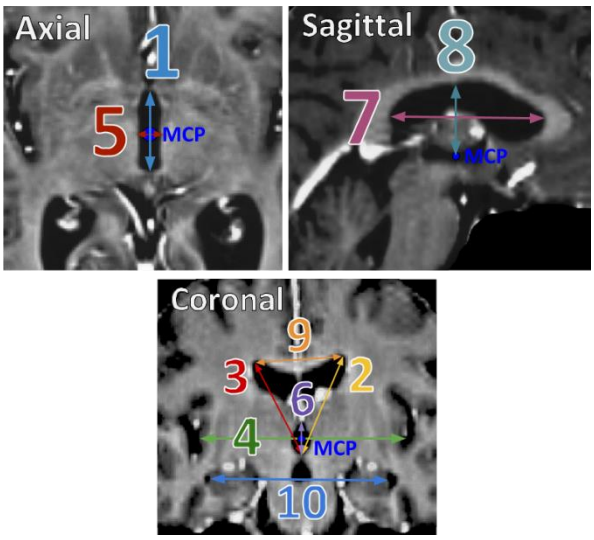

Fig. 4. Set of selected measurements

This set of dimensions were accounted as the most representative of the brain morphology and spatial distribution for each patient. That is, for example, if a set of dimensions in the lateral direction is found to be above the average, it is expected that the STN location is also more shifted laterally than normal.

C. Features model

With the features approach, it is assumed that the information extracted from the medical image doesn't have to be necessarily quantified by anatomical principles. As such, this second model considers information regarding voxel intensity averages and the 3 directional image gradients from a set of small cubic volumes located around the MCP. The adoption of this kind of features was inspired by a study which was focused on the identification of the human hand configuration using an ultrasound image of a sectional plane of the forearm [11].

Figure 5 shows a scheme representing the brain ventricular system and the interest volume, chosen for the image features extraction. That volume was then subdivided into 18 smaller volumes (fig. 6). As the main volume position and size was defined using the posterior and anterior commissure points, the same position and orientation were assured for all the patients from whom the information was acquired. The volume dimensions were 40mm in the lateral direction, 50mm in the vertical direction and 2 times de AC-PC distance in the anterior-posterior direction. The division was made the same way for all the patients, 2 divisions over the lateral-medial direction, and 3 divisions over the vertical and anterior-posterior directions. From these 18 smaller volumes were extracted a total of 72 features for each patient.

D. Linear Regression

The linear regression method consists of finding the optimal regression coefficients represented as β in the following expression:

$$y_i = \beta_1 x_{i1} + \cdots + \beta_p x_{ip} + \varepsilon_i = \mathbf{x}_i^{\mathrm{T}} \boldsymbol{\beta} + \varepsilon_i \qquad (1)$$

In this expression, y_i stands for the response variable or measured variable, $\boldsymbol{\beta}$ is the vector of regression coefficients, of p dimention, $\mathbf{x}_i^{\mathrm{T}}$ represents the vector of input or predictor variables for a given data observation i (in the study context, each observation is given by a patient) and finally ε_i stands for the estimation error for the observation i. The p dimension is equal to the number of input variables for each model.

The goal of the learning process in a linear regression is, therefore, to obtain the combination of estimation parameters β that minimizes the estimation error ε_i for all the observations from the learning dataset. The most widely used method for this minimization is the least squares method. This method, defines the learning goal as the minimization of the function (in the case of a linear regression):

$$S = \sum_{i=1}^{N} \left(y_i - \beta_0 - \beta_1 x_{i1} - \cdots - \beta_p x_{ip} \right)^2 \qquad (2)$$

Which is described as the sum of squared estimation errors for all the learning dataset observations. This function is quadratic with the regression parameters, therefore, an analytical solution

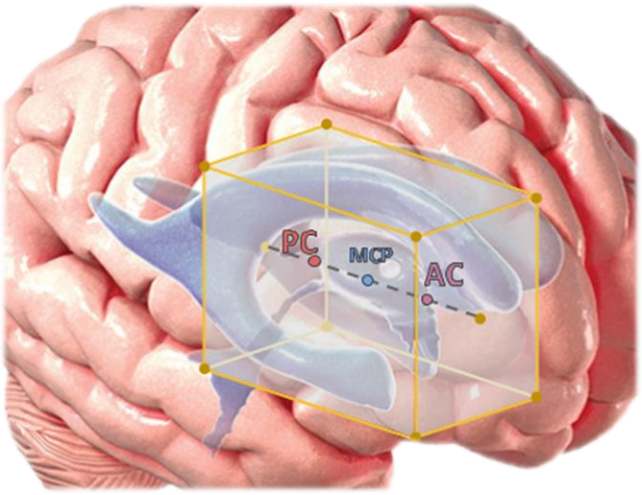

Fig. 5. Positioning of the main volume inside which the smaller ones are contained [15]

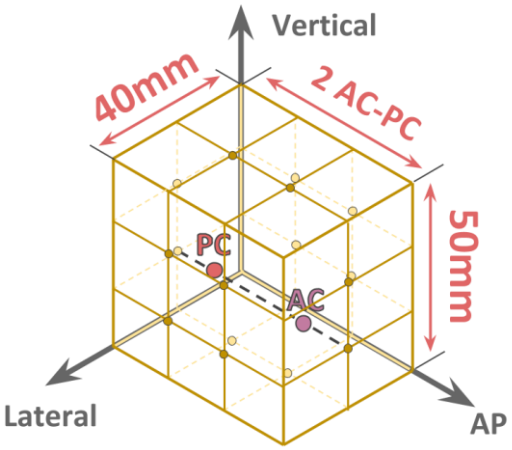

Fig. 6. Main volume partition in 18 smaller volumes

for this minimization problem is easily obtained. The minimization problem unique solution is obtained by solving the following matrix equation:

$$\widehat{\boldsymbol{\beta}} = (\mathbf{X}^{\mathrm{T}}\mathbf{X})^{-1}\mathbf{X}^{\mathrm{T}}\boldsymbol{y} \tag{3}$$

Where $\widehat{\boldsymbol{\beta}}$ stands for the optimal vector of regression parameters.

E. Support Vector Machine

The learning method that uses a SVM may be more precisely described as a nonlinear regression using a support vector machine. Therefore, it can be divided in the search for a solution for the optimization problem and the application of a nonlinear mathematical function (known as the kernel function) which shapes the original problem into a nonlinear problem. For a best understanding of the details of the nonlinear regression method it is required to first introduce the simpler linear regression using an SVM problem. This problem takes the linear model given by the function:

$$f(\mathbf{x}) = \boldsymbol{\beta}\mathbf{x}^{T} + \boldsymbol{b} \tag{4}$$

The purpose of the support vector machine is to find the function $f(\mathbf{x})$ that deviates from the response vector $\mathbf{y}_n$ by value smaller than ε for each training observation form $\mathbf{x}$ (predictor variables). The optimization problem is more easily solved in its Lagrange formulation given by the minimization of the function [12]:

$$L(\alpha) = \frac{1}{2}\sum_{i=1}^{N}\sum_{j=1}^{N}(\alpha_i - \alpha_i^*)\left(\alpha_j - \alpha_j^*\right)\mathrm{x}_i^{\mathrm{T}}\mathrm{x}_j + \varepsilon\sum_{i=1}^{N}(\alpha_i + \alpha_i^*) + \sum_{i=1}^{N} y_i(\alpha_i - \alpha_i^*) \tag{5}$$

Subject to:

$$\sum_{n=1}^{N}(\alpha_n - \alpha_n^*) = 0 \tag{6}$$

$$\forall n : 0 \le \alpha_n \le C \tag{7}$$

$$\forall n : 0 \le \alpha_n^* \le C \tag{8}$$

In which α_n and α_n^* are the Lagrange multipliers and C is real positive number that controls the penalty over the observations that deviate by a value bigger than the boundary value (ε). The β parameters vector can be described as a linear combination of the training dataset:

$$\beta = \sum_{n=1}^{N}(\alpha_n - \alpha_n^*)\mathrm{x}_n \tag{9}$$

Hence, the function $f(x)$ is given by:

$$f(x) = \sum_{n=1}^{N}(\alpha_n - \alpha_n^*)(\mathrm{x}_n^{\mathrm{T}}\mathrm{x}) + b \tag{10}$$

For the regression to be nonlinear, it is introduced a small modification of the Lagrange formulation by the replacing the dot product $\mathrm{x}_1^{\mathrm{T}}\mathrm{x}_2$ by some nonlinear kernel function $G(\mathrm{x}_1, \mathrm{x}_2) = \langle\phi(\mathrm{x}_1), \phi(\mathrm{x}_2)\rangle$, where $\phi(\mathrm{x})$ represents a transformation that maps x into a high-dimensional space [13]. This kernel function can be arbitrarily chosen as any nonlinear function and, with its application, it will never be required to compute that high-dimensional transformation as it is only necessary to calculate the dot product of predictor variables transformed by ϕ to obtain the optimal solution. This solution is, however, given in the variable space transformed by $\phi(\mathrm{x})$. This method if often referred as kernel trick

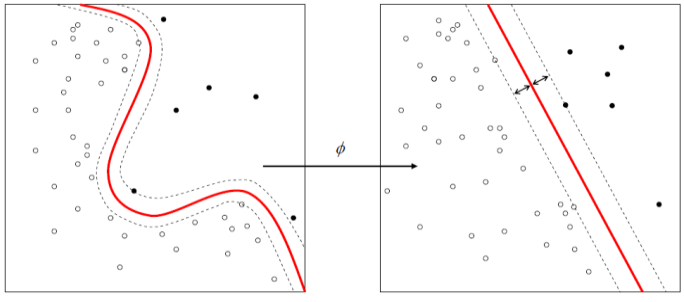

Fig. 7. Kernel trick visualization[16]

F. Models validation

For the quantification of the errors obtained with the different models, the Euclidian distance between the estimation and real stimulation target was decomposed in the error orthogonal to the trajectory of the electrode and the remaining error within the trajectory. This decomposition is due to the different implications that this two forms of error have in the problem context. As mentioned above, 5 micro electrodes, used to correct the targeting estimation made in the planning, are introduced in the planned trajectory during the surgery. These electrodes are only spaced by 2.5mm (2mm plus the electrode diameter) in directions orthogonal to the trajectory, on the other hand, the explored depth of the trajectory has an average size of 7mm. Therefore, errors within the trajectory of the electrode are easily more tolerated than the errors on the plane orthogonal to the electrode. Hence, for the conceptualization of a total error of a model, it is desirable that the orthogonal error suffers from a bigger penalty than the error within the trajectory. The proposed total error of a model is calculated as:

$$E = \sqrt{E_O^2 + 0.16E_T^2} \qquad (11)$$

Where E_O stands for the orthogonal error and E_T the error within the trajectory. Using the above expression to calculate the total error of a model, the E_O is weighted as 1 and E_T as 0.4.

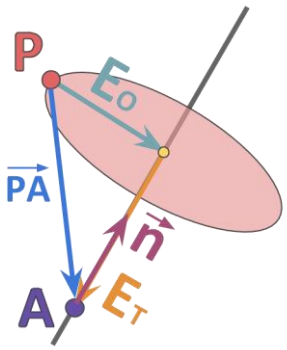

Fig. 8. Auxiliary vector necessary to the computation of the two error components

Consequently, for the decomposition of the Euclidian error in this two components, additionally to the active contacts location, the electrode trajectory directions were also acquired for all the patients considered in this study.

To obtain the two components of the error for a given model, a cross-validation method was implemented with a group of test with 20% of the total observations. This observations division into training group and test group is done randomly and the process is repeated 1000 times for statistical validity assurance (see fig. 9). From each patient of the test group, both the orthogonal and within the trajectory errors are computed. In the test group, mean and standard deviation are obtained for the two components of the error. Hence, the mean errors, and corresponding standard deviations for a given model, are obtained calculating the means of these two parameters for all the 1000 test groups.

G. Feature extraction

With a principal component analysis, the dimensionality reduction is achieved by a statistical procedure that obtains an orthogonal transformation which takes the original (possibly) correlated variables, and returns a set of new variables without correlation between each other. These new variables are also all intrinsically orthogonal with each other and are arranged by a score. The variable with the highest score is the one whose direction has the highest variance in the population, since this score is the percentage of information that each variable explains. The dimensionality reduction is done by the rejection of the variables that have the lower scores, and therefore, are negligible. The method applied in this study, rejected all variables with a score lower than 2%.

H. Feature selection

For reducing the dimensionality of the data using feature selection, a genetic algorithm was implemented. This solution, in contrast to the solution applied in feature extraction, depends of the model that is under consideration. This genetic algorithm searches for solutions in all the combinatory space of variables, evaluating the effect of each combination on each model and learning method by the computation of the total error of the model.

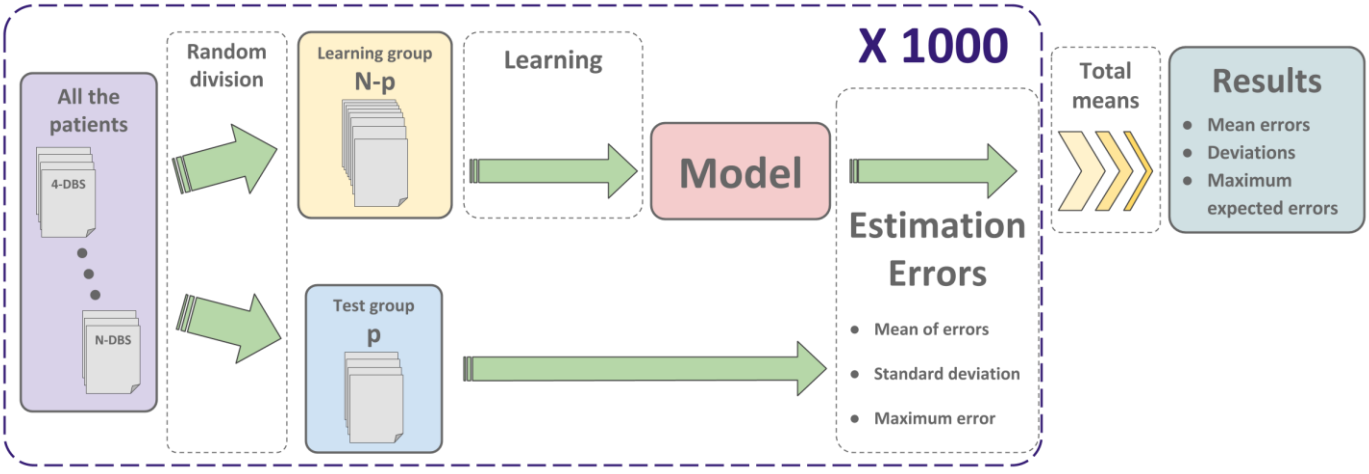

Fig. 9 – Schematization of the cross-validation method used

The algorithm implementation considers that each solution/subject stands for a combination of variables, and associated with it, a score is calculated corresponding to the quality of the model given by the total error. In order to accelerate the process, this error is obtained using a leave-one-out approach (special case of the cross-validation method where just one patient is considered for the test group and the number of repetitions is equal to the number of patients considered). The first generation of the algorithm is created randomly with a size of each solution also determined randomly. This way, solutions with the minimum number of variables can be obtained. After that, the scores are computed for all subjects of the generation, then a selection of the best fitted subjects is done. The new generation subjects are created from the selected members. The crossover is done considering that both solutions created may have different dimensions than the two that originated them. The information equal in the two original solutions is replicated into both the new solutions, as for the remaining information, it is divided randomly between the two new solutions. The mutation process is done by adding a new variable, randomly selected from the set of variables that aren´t part of the solution.

The stopping criteria used, was that the best solution of each generation has not improved for over a given number of generations.

I. Developed software

For the construction of the models described previously, it was necessary to find a software tool that was able to provide all the functionalities demanded by this study, which were: reading files in the DICOM format, image registration, volume orientation with the identification of specific image references, dimension measurement and feature extraction from specific volumes. It wasn´t possible to find such a software, so it had to be developed one which allowed the use of all the necessary tools, inside the same neuro-navigation environment. All this tools were developed over a graphical user interface with the MATLAB® v. R2016a software. The created software is divided in 3 parts:

- Active contacts localization module – Using an image registration algorithm, T1-weighted MRI and post-surgery CT are presented simultaneously, which enables to see the electrodes location relative to the brain structures. The next step is the acquisition of the location of active contacts relative to the MCP and the directions of the electrodes trajectories;
- Anatomical measurements module – Using T1-weighted MRI, measurements might be extracted directly from the visualization planes;
- Features extraction module – Once more, using the T1-weighted MRI, an interest volume is selected and subdivided. From each volume resulting from the division, 4 features, defined previously, are automatically obtained.

The graphical environment is very similar in each of the modules. The three visualization planes (axial, sagittal and coronal) are presented side-by-side. The navigation is allowed by moving each intersection plane over his normal direction.

III. Results

For the comparison of the obtained results with some kind of reference, planning errors were computed for all the patients using the STN location estimations, produced by the neurosurgery team form the hospital and recorded in the planning sheets. Another model was developed using only the information relative to the location of all the active contacts for all the patients. The model was obtained as a statistical atlas – a mean of the location of various patients active contacts was projected onto a new patient, consisting of an estimation for that same patient. From that estimation, both error components are obtained. For this test model, the same cross-validation method used for computing all the models errors, was applied.

The set of tested models has two variations on the approaches side, the measurements approach and the features approach, plus two different learning methods, and first or both implants are considered. Finally, there are the three dimensionality reduction variants, data without reduction, data obtained from feature selection and data obtained after feature extraction. Due to the large extension of models tested, some code names were endorsed for each model for an easy identification during results presentation (see Table I). Models were also divided in two groups, for results presentation. The first one includes all the models without dimensionality reduction (WR) and the second one incorporates the models from the two kinds of dimensionality reduced models.

TABLE I

SET OF TESTED MODELS

Models		Measurements		Features		Group
		RL	*SVM*	*RL*	*SVM*	
WR	*1st Side*	Med_RL1	Med_SVM1	Fea_RL1	Fea_SVM1	*1*
	Both	Med_RL2	Med_SVM2	Fea_RL2	Fea_SVM2	
FE	*1st Side*	EMed_RL1	EMed_SVM1	EFea_RL1	EFea_SVM1	*2*
	Both	EMed_RL2	EMed_SVM2	EFea_RL2	EFea_SVM2	
FS	*1st Side*	SMed_RL1	SMed_SVM1	SFea_RL1	SFea_SVM1	
	Both	SMed_RL2	SMed_SVM2	SFea_RL2	SFea_SVM2	

J. Models without dimensionality reduction

From the first group, the 2 best models were selected by the comparison of the total error for all the 8 models of this group. The results are presented in Table II, where the results for the planning errors and the test model were also included for comparison.

TABLE II

MEAN ERRORS, STANDARD DEVIATIONS AND TOTAL ERROR FROM THE 2 BEST MODELS FROM GROUP 1, PLANNING AND TEST MODEL

Errors (mm)	Orthogonal	Trajectory	Total Error
	Mean ± Std	*Mean ± Std*	
Planning	1,55 ± 1,16	2,67 ± 1,84	1,88
Test Model	1,62 ± 0,73	2,48 ± 1,67	1,90
Med_SVM2	1,52 ± 0,79	2,22 ± 1,42	1,76
Fea_SVM1	1,59 ± 0,77	2,30 ± 1,58	1,84

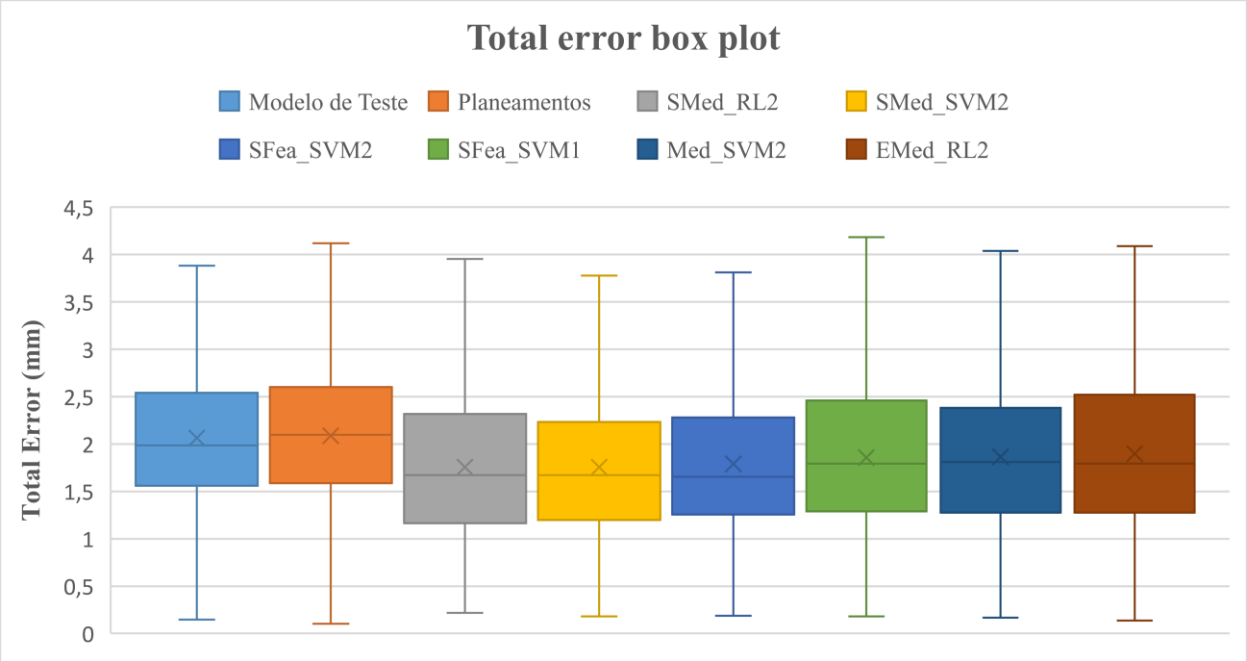

Fig. 10. Box plot graph of the total errors distributions from all the models presented in this study

K. Models from data with dimensionality reduced

For the second group, the 4 best models were selected form the total 16 by the comparison of the total errors. These models results are shown in Table III

TABLE III

MEAN ERRORS, STANDARD DEVIATIONS AND TOTAL ERROR FROM THE 4 BEST MODELS FROM GROUP 2, PLANNING AND TEST MODEL

Errors (mm)	**Orthogonal** *Mean ± Std*	**Trajectory** *Mean ± Std*	**Total Error**
Planning	1,55 ± 1,16	2,67 ± 1,84	1,88
Test Model	1,62 ± 0,73	2,48 ± 1,67	1,90
SMed_RL2	1,36 ± 0,75	2,28 ± 1,54	1,63
SMed_SVM2	1,41 ± 0,75	2,19 ± 1,38	1,66
SFea_SVM2	1,41 ± 0,73	2,25 ± 1,48	1,67
EMed_RL2	1,44 ± 0,85	2,52 ± 1,40	1,76

L. Comparison of all the models obtained

To facilitate the comparison between the results obtained with the different models, a box plot graph was created with the total errors obtained for the 6 best models (fig. 10). Additionally, a statistical t-Test and a statistical *F*-Test were performed, with a 5% significance level, in order to test the hypothesis of equality of means and variances of the total errors, respectively, of the 6 models and the test model. Tables IV and V show the results obtained from these tests.

TABLE IV

T-TEST OF THE HYPOTHESIS OF EQUAL MEAN. R MEANS THAT THE HYPOTHESIS WAS REJECTED

t-Test (5%)	**H**	***p*-value**	**CI**
Test Model vs SMed_RL2	R	4,88e-61	[0,25 0,31]
Test Model vs SMed_SVM2	R	3,53e-64	[0,25 0,32]
Test Model vs SFea_SVM2	R	3,88e-45	[0,20 0,27]
Test Model vs Fea_SVM1	R	3,50e-21	[0,14 0,21]
Test Model vs Med_SVM2	R	1,25e-23	[0,14 0,21]
Test Model vs EMed_RL2	R	4,57e-16	[0,11 0,18]

TABLE V

F-TEST OF THE HYPOTHESIS OF EQUAL VARIANCE. R MEANS THAT THE HYPOTHESIS WAS REJECTED

***F*-Test (5%)**	**H**	***p*-value**	**CI**
Test Model vs SMed_RL2	-	0,296	[0,97 1,10]
Test Model vs SMed_SVM2	-	0,199	[0,98 1,11]
Test Model vs SFea_SVM2	R	0,0013	[1,04 1,18]
Test Model vs Fea_SVM1	R	1,11e-25	[0,67 0,76]
Test Model vs Med_SVM2	-	0,276	[0,91 1,03]
Test Model vs EMed_RL2	R	0,018	[0,87 0,98]

The first conclusion that can be drawn for the results obtained from the t-Test is that all the presented models obtained total errors with mean significantly different from the mean of the total error obtained with the test model. From the *F*-Test, one can conclude that only the models SFea_SVM2, Fea_SVM1 and EMed_RL2 obtained total errors with variance significantly different from the variance of the total errors from the test models. On the other hand, the variances of the total errors obtained for the models SMed_RL2, SMed_SVM2 and Med_SVM2 weren't significantly different from the variance of the total errors obtained with the test model.

IV. Discussions and Conclusions

The linear regression model, obtained from the anatomical measurements and that considers both sides of the implants was the model that obtained the best results in this study. This suggests that there might exist a linear relation between some dimensions of encephalic structures and the coordinates of the location of the STN, relative to the MCP. Generally speaking, the feature selection procedure was the one that originated the best results.

The most important aspect to have in mind, for all the models variations, is the number of parameters that has to be estimated for each model construction. This parameter number is deeply related with the number of variables (or dimensionality) of the entry data for each model. A correct learning should be provided with a sufficiently big number of observations relative to the number of estimation parameters of each model. However, it is known that, in the case of this study, the observations number (36 implantations considering both sides, 18 considering only the first side) is relatively small. Therefore, it becomes really hard to have a statistical validity for the estimation of all the parameters. Considering a normal distribution of the input data, for a statistically valid estimation of a model with just one estimation parameter, it would require, at least, 30 data observations. Therefore, good training conditions are not met, as the input data has dimensionality superior to one variable. Thus, the obtained models are not that good at finding the relation between the variability in the input data and the variability of the STN coordinates (which is the assumption considered to be true for the implementation of the predictive model with the structure proposed). Even so, for some models, improvement was achieved relative to the test model, indicating that these models could, somehow, use the information in the measurements/features, obtained from the image of each patient, to give a better estimation of the STN location than simpler methods. Models that obtained the best results are from the group where feature selection was performed. That could be related with the high degree of dimensionality reduction of this method. Hence, for these models, parameter estimation was preformed more accurately.

Another important aspect is that both the measurements and features approaches originated models with quality comparable to the manual predictions produced by the surgical planning. The SVM learning method was responsible for a larger amount of models with satisfactory results, however, the model with the lowest total estimation error was obtained by a linear regression method.

Finally, one can say that a big limitation of the quality of the obtained results was the small number of observations in the data considered for this study. Nevertheless, by the observation of the obtained results, it is reasonable to say that a predictive model implementation for the STN targeting based on the information extracted from the patient MRI is possible, and it is likely to obtain results with a superior quality than the manual estimations produced in the surgical planning. Another way of validating the models developed is by looking at the orthogonal errors obtained for the best models presented. These mean errors are smaller than the 2.5mm limit dictated by the microelectrodes spacing. Even if the standard deviation is added to the normal error, in most cases, it is still inside the prospection volume of the microelectrodes.

A. Future work

For the continuity of the work developed, with the purpose of still improving the quality of the implemented models, the following suggestions are made:

- Collecting more observations in order to increase the dataset considered in the learning methods;
- Implementation of an automatic segmentation procedure to extract the measurements automatically;
- Optimization of the dimensions, positions and division of the main volume from which are extracted the features. It would also be important to test another type of features besides means and directional gradients;
- Implementation of an automatic segmentation method for the segmentation of the complete ventricular system, from which is possible to obtain more concrete information about the morphology and spatial distribution of each patient brain;
- Include, in the predictive model, an estimation of the electrode trajectory direction using the information from previous implanted electrodes and having as input information from the image collected from a volume around the electrode trajectory;
- Direct comparison, for the same group of patients, of the predictive model for the automatic targeting of the STN and the non-rigid registration methods widely used by the medical community.

References

[1] M. Kringelbach, N. Jenkinson, S. Owen e T. Aziz, "Translational principles of deep brain stimulation," Nature Reviews Neuroscience, 2007.

[2] C. Hammond, R. Ammari, B. Bioulac e L. Garcia, "Latest view on the mechanism of action of deep brain stimulation," Mov Disord, 2008.

[3] J. M. Bronstein, M. Tagliati, R. L. Alterman e A. M. Lozano, "Deep Brain Stimulation for Parkinson Disease, An Expert Consensus and Review of Key Issues," JAMA Neurology, 2011.

[4] F. J. S. Castro, C. Pollo, O. Cuisenaire, J.-G. Villemure e J.-P. Thiran, "Validation of experts versus atlas-based and automatic registration methods for subthalamic nucleus targeting on MRI," Int J CARS, 2006.

[5] B. Bejjani, D. Dormont, B. Pidoux, J. Yelnik, P. Damier, I. Arnulf, A. Bonnet, C. Marsault, Y. Agid, J. Philippon e P. Cornu, "Bilateral subthalamic stimulation for Parkinson's disease by using three-dimensional stereotactic magnetic resonance imaging and electrophysiological guidance.," Journal of Neurosurgery, 2000.

[6] P. Starr, “Placement of deep brain stimulators into the subthalamic nucleus or Globus pallidus internus: technical approach.,” [PubMed: 12890973], 2002.

[7] M. Rodriguez-Oroz, M. Rodriguez, J. Guridi, K. Mewes, V. Chockkman, J. Vitek, M. DeLong e J. Obeso, “The subthalamic nucleus in Parkinson's disease: somatotopic organization and physiological characteristics.,” [PubMed: 11522580], 2001.

[8] P. Starr, C. Christine, P. Theodosopoulos, N. Lindsey, D. Byrd, A. Mosley e W. Marks, “Implantation of deep brain stimulators into the subthalamic nucleus: technical approach and magnetic resonance imaging-verified lead locations.,” Journal of Neurosurgery, 2002.

[9] J. Voges, J. Volkmann, N. Allert, R. Lehrke, A. Koulousakis, H. Freund e V. Sturm, “Bilateral high-frequency stimulation in the subthalamic nucleus for the treatment of Parkinson disease: correlation of therapeutic effect with anatomical electrode position.,” Journal of Neurosurgery, 2002.

[10] M. Zonenshayn, A. Rezai, A. Mogilner, A. Beric, D. Sterio e P. Kelly, “Comparison of anatomic and neurophysiological methods for subthalamic nucleus targeting.,” [PubMed: 10942001], 2000.

[11] D. S. González e C. Castellini, “A realistic implementation of ultrasound imaging as a human-machine interface for upper-limb amputees,” Front Neurorobot, 2013.

[12] "Understanding Support Vector Machine Regression" [Online]. Available: https://www.mathworks.com/help/stats/understanding-support-vector-machine-regression.html [Accessed 20 June 2016].

[13] T. Hofmann, B. Scholkopf e A. J. Smola, “Kernel Methods in Machine Learning,” 2008.

[14] "MedicalExpo" [Online]. Available: http://www.medicalexpo.com/prod/inomed-medizintechnik/product-68872-442506.html [Accessed 15 September 2016].

[15] "Epic Studios Inc." [Online]. Available: http://epicstudios.com/?p=4847 [Accessed 2 March 2016].

[16] Z. Wojciech, M. B. Blaschko, P. K. Mudigonda, H. Hung e S. Nguyen, “Modeling the Variability of Eeg/meg Data through Statistical Machine Learning Supervisor's Statement Subject Classification,” 2012.

[17] "Deep Brain Stimulation" [Online]. Available: https://en.wikipedia.org/wiki/Deep_brain_stimulation [Accessed 28 February 2016].